American Mineralogist, Volume 79, pages 719–736, 1994

Role of fluid flow in the contact metamorphism of siliceous dolomitic limestones

JOHN M. FERRY
Department of Earth and Planetary Sciences, Johns Hopkins University, Baltimore, Maryland 21218, U.S.A.

ABSTRACT

One-dimensional models predict the spatial distribution of mineral assemblages developed in siliceous dolomitic limestones during three conditions of contact metamorphism and fluid-rock interaction: (1) rock containing a fixed porosity filled with stagnant CO_2-H_2O fluid, (2) horizontal fluid flow in the direction of increasing temperature, and (3) horizontal flow in the direction of decreasing temperature. For a given pressure, temperature profile, and rock composition, and assuming local mineral-fluid equilibrium, stable assemblages may be mapped on diagrams of distance from the contact vs. fluid amount (porosity, ϕ, or time-integrated flux, q, as appropriate). The topology of the diagrams differs for the three cases of fluid-rock interaction. Observed mineral assemblages in specific aureoles therefore may be interpreted in terms of the amount and direction of fluid flow (if any). Review of seven case studies of contact-metamorphosed siliceous dolomitic limestones indicates that unless $\phi > 14\%$, fluid flow occurred in each instance. No universal statements, however, may be made about the geometry of flow. The outer portions of five aureoles (Alta, Utah; Beinn an Dubhaich, Scotland; Boulder, Montana; Kasuga-mura, Japan; and Marysville, Montana) contain a mineralogical record consistent with horizontal fluid flow in the direction of increasing temperature with $q \approx 10$–800 mol/cm^2. Two localities (Alta and Beinn an Dubhaich) show evidence for flow in the direction of decreasing temperature in the innermost portion of the aureole with $q < 1300$ mol/cm^2. In one aureole (Elkhorn, Montana), fluid probably flowed horizontally down-temperature in the outer portion ($q \approx 35$–165 mol/cm^2) and upward near the contact. Results emphasize that mineral assemblages in metacarbonate rocks are controlled not only by temperature, pressure, rock composition, and fluid composition but also by the amount and direction of fluid flow.

INTRODUCTION

Because of their chemical simplicity, siliceous dolomitic limestones play a key role in efforts to understand the development of mineral assemblages in metamorphic rocks. The dependence of mineral assemblage on bulk rock composition, pressure, temperature, and fluid composition has been appreciated for more than two decades. The importance of fluid dynamics—whether fluid is flowing or not, the direction of flow if it occurs, and the amount of fluid—has been recognized only recently. This report systematically and quantitatively evaluates how the amount and direction of fluid flow controls the development of mineral assemblages during contact metamorphism of siliceous dolomitic limestones. Results are applied to published field studies of carbonate rocks in contact aureoles.

METHODS, ASSUMPTIONS, AND INPUT DATA

General statement

The primary mineralogical records of contact metamorphism are the assemblages encountered along a transect through the aureole radial to the pluton. Such a transect is represented in this study by the distance coordinate of several one-dimensional models. The sequence and spatial relations among assemblages along the coordinate depend on bulk rock composition, pressure, temperature, fluid composition, fluid amount, and the direction of fluid flow (if flow occurs). To isolate the effects of fluid amount and flow direction, several of these variables were held constant or were constrained. Computations were restricted to two rock compositions. Pressure was set at a constant value. Temperature along the distance coordinate was defined by a steady-state temperature profile. Fluid composition was specified by mineral-fluid equilibrium. With these constraints, the stable assemblage of minerals was computed and mapped onto a diagram of distance along the transect vs. fluid amount.

Three models of fluid dynamics are explored. The first uses the assumption that the rock contains a fixed porosity filled with stagnant fluid. Porosity represents fluid amount. The chemical effect of whatever fluid transport is required to maintain constant porosity is considered negligible. Computational and field studies, however, indicate that many instances of contact metamorphism involve fluid flow with a large horizontal component in the direction of either increasing or decreasing temperature (e.g., Norton and Knight, 1977; Hanson, 1992) and that

0003–004X/94/0708–0719$02.00

rocks chemically react with the flowing fluid (e.g., Labotka et al., 1988; Ferry and Dipple, 1992). The other two models represent metamorphism with horizontal fluid flow in the direction of either increasing (up-temperature) or decreasing temperature (down-temperature). Fluid amount is tracked by time-integrated flux. Because subhorizontal surfaces are typically exposed in contact aureoles, observed sequences of assemblages and their spatial relations in specific contact aureoles can be interpreted directly with the calculated results. Although no models for vertical flow were developed, evidence for vertical flow in some aureoles is discussed.

Model rock compositions and protolith mineral assemblage

One rock composition considered corresponds to a mixture of dolomite (90% by volume) and quartz (10%) that is like the protoliths to many contact-metamorphosed siliceous dolomites (e.g., Bowman and Essene, 1982; Holness, 1992). Another composition corresponds to a mixture of dolomite (34.745%), quartz (30.643%), calcite (19.933%), and potassium feldspar (14.679%) that is like protoliths to metamorphosed impure carbonate rocks in the Boulder and Marysville aureoles, Montana (Rice, 1977a, 1977b; Rice and Ferry, 1982).

Pressure and temperature

Pressure was assumed to be 1 kbar, a value representative of many instances of contact metamorphism. Temperature along the distance coordinate of the models corresponds to a typical horizontal, peak metamorphic temperature profile through a contact aureole radial to the pluton:

$$T\ (^{\circ}\mathrm{C}) = 150 + 500\mathrm{e}^{-0.6932Z\ (\mathrm{km})} \qquad (1)$$

where Z is measured outward from a value of zero at the contact. Equation 1 corresponds to a temperature of 650 °C at the contact, 400 °C at a distance of 1 km, and 150 °C far outside the aureole. The profile defined by Equation 1 is consistent with those produced by the conductive cooling of intrusions (Furlong et al., 1991).

The thermal evolution of the model aureole can be roughly calculated using Equation 4-113 of Turcotte and Schubert (1982) and the same boundary conditions that define Equation 1 (T = 650 °C at the contact; T = 150 °C far from the pluton). For a diffusivity of 0.01 cm²/s, the temperature calculated from Equation 4-113 differs after 35000 yr at Z < 1200 m by ≤15 °C from that defined by Equation 1. Equation 1 represents the peak thermal state of the aureole following heating that lasts ≈35000 yr and then stops. Equation 4-113 further predicts that the temperature at a representative position like Z = 400 m lies within 50 °C of the peak value for 55% of the heating interval and that the temperature gradient at the same time changes by <30% (relative). The common preservation of high-temperature minerals in contact aureoles indicates that significant mineral reaction usually does not occur after peak temperatures are reached. Cooling of the aureole therefore can be safely ignored in models for the development of prograde mineral assemblages. Although temperature increases and decreases in real contact aureoles, use of Equation 1 in the calculations is justified because it approximates the thermal structure of the model aureole for a significant portion of the time that prograde mineral-fluid reactions would be active.

In any case, the use of a time-dependent temperature profile would require consideration of complexities far beyond the scope of this study. First, the effects of reaction kinetics would have to be included, otherwise minerals would reequilibrate during cooling to low-temperature assemblages not commonly observed in aureoles. Second, a hydrologic model would be required to couple correctly Darcy flux with evolving temperature. A realistic time-dependent model therefore would have to specify numerous poorly constrained factors including the form of reaction rate laws (linear or nonlinear), rate constants and their temperature dependence, grain size, the spatial distribution of fluid in rock, the time- and space-dependence of permeability, and the driving force for fluid flow. One strength of models that specify a steady-state temperature with Equation 1 is that they characterize important aspects of metamorphic fluid flow independent of a detailed understanding of the physical mechanisms of heat and fluid transfer.

Minerals, fluid, and mineral-fluid equilibria

Minerals considered were dolomite (Dol), quartz (Qtz), calcite (Cal), potassium feldspar (Kfs), talc (Tlc), phlogopite (Phl), tremolite (Tr), diopside (Di), forsterite (Fo), wollastonite (Wo), periclase (Per), and brucite (Brc). Composition and thermodynamic properties were taken from Berman (1988, updated by personal communication, August, 1990). Fluid was assumed to be a CO_2-H_2O mixture that obeys the equation of state of Kerrick and Jacobs (1981). Figures 1 and 2 illustrate all possible stable mineral reactions in the two rock compositions involving these minerals and CO_2-H_2O fluid at 1 kbar and T = 350–650 °C. Other equilibria required by Schreinemakers analysis have been omitted for clarity. For ease in computation of X_{CO_2} and $(\partial X_{CO_2}/\partial T)_P$, T-X_{CO_2} points on each curve were fit to a polynomial expression that typically reproduces values of X_{CO_2} calculated from Berman's data with a maximum deviation of ±0.005.

Lasaga and Rye's (1993) model for coupled fluid flow and kinetically controlled metamorphic mineral reactions predicts near-equilibrium conditions for a plausible range of flow velocities and reaction kinetics, in harmony with a variety of evidence for a close approach to equilibrium in specific case studies of metamorphism (Baumgartner and Ferry, 1991). For other plausible ranges, their model predicts significant disequilibrium that would effect widespread development of mineral assemblages with phase rule variance ≤1. Low-variance assemblages do not have a widespread distribution in carefully studied contact aureoles (e.g., Rice, 1977a, 1977b). Calculations therefore

were made with the assumption that fluid compositions are defined by mineral-fluid equilibrium.

Change in rock volume by reaction

In all calculations, changes in rock volume caused by mineral reactions were ignored. Explicit consideration of the effect would have made the computations significantly more difficult without changing results qualitatively.

Models for contact metamorphism

No fluid flow

General procedure. The first model considers rock containing a fixed fluid-filled porosity and establishes mineralogy as a function of porosity (ϕ) and position along the distance coordinate (Z). Initial pore fluid composition was set at $X_{CO_2} = 0.05$; final results are qualitatively the same provided $X_{CO_2} < \approx 0.5$. For a given value of porosity, rock at each position Z was heated to a maximum value specified by Equation 1. The progress of mineral reactions was tracked as temperature increased, and the final (peak) mineral assemblage was plotted on a diagram of ϕ vs. Z. As shown by Equation 2, below, progress of prograde reactions, and hence mineral assemblage at each position Z, depends on porosity. The calculation therefore was performed for porosities in the range 0–50%. Values of $\phi > 50\%$ were ignored because the material would then be a slurry rather than a rock (Marsh, 1981).

Progress of a mineral-fluid reaction (ξ) at each position Z was computed from an equation obtained by generalizing the differential equation in Appendix 1 of Labotka et al. (1984) to consider decarbonation-dehydration reactions and integrating it:

$$\xi = -\frac{V_p}{\nu_{CO_2}\cdot V_{CO_2} + \nu_{H_2O}\cdot V_{H_2O}} \cdot \ln \frac{\nu_{CO_2}\cdot V_{CO_2} - (\nu_{CO_2}\cdot V_{CO_2} + \nu_{H_2O}\cdot V_{H_2O})y^f_{CO_2}}{\nu_{CO_2}\cdot V_{CO_2} - (\nu_{CO_2}\cdot V_{CO_2} + \nu_{H_2O}\cdot V_{H_2O})y^0_{CO_2}} \quad (2)$$

where ν_{CO_2} and ν_{H_2O} are the stoichiometric coefficients of CO_2 and H_2O in the reaction, V_{CO_2} and V_{H_2O} are the molar volumes of pure CO_2 and H_2O, y_{CO_2} is the volume fraction of CO_2 in fluid at the beginning (0) and end (f) of reaction, and V_p is the volume of pores per unit volume of minerals to which ξ refers. Porosity $\phi = V_p/(V_p + 1)$. Equation 2 is exactly correct for the limiting case of reactions involving only CO_2 or H_2O and is only accurate in the case of reactions involving both CO_2 and H_2O to the extent that $(\nu_{CO_2}V_{CO_2})/[(\nu_{CO_2}V_{CO_2}) + (\nu_{H_2O}V_{H_2O})]$ is constant over the limits of integration. The maximum change in $(\nu_{CO_2}V_{CO_2})/[(\nu_{CO_2}V_{CO_2}) + (\nu_{H_2O}V_{H_2O})]$ over any of the limits considered was 0.6%, and in most cases the change was <0.2%. Equation 2 is an adequate approximation for reactions involving both CO_2 and H_2O. Equation 2 differs from Equation 2 of Ferry (1991) because of a typographical error in the latter. Molar volumes were computed from the Kerrick and Jacobs (1981) equation of state at $P = 1$ kbar and T of interest. Values of y_{CO_2} were calculated as $(V_{CO_2})(X_{CO_2})/[(V_{CO_2})(X_{CO_2}) + (V_{H_2O})(1 - X_{CO_2})]$.

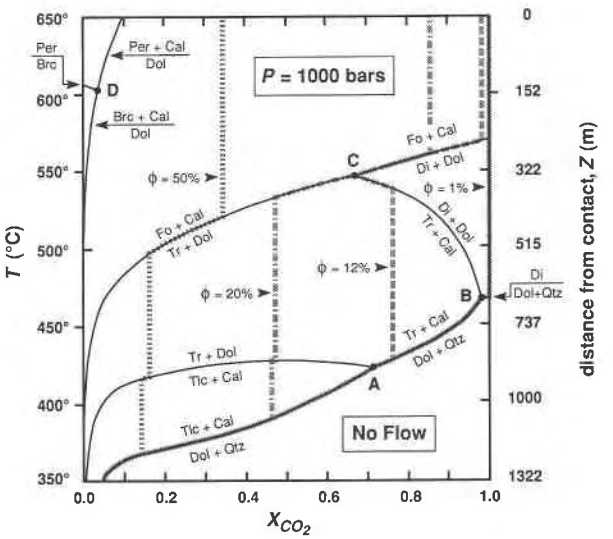

Fig. 1. Stable reactions in the model Dol + Qtz rock involving Dol, Qtz, Tlc, Cal, Tr, Di, Fo, Per, Brc, and CO_2-H_2O fluid at $P = 1$ kbar and $T = 350$–650 °C calculated from data in Berman (1988) and the equation of state for CO_2-H_2O fluid of Kerrick and Jacobs (1981). Other reactions possible in different rock compositions were omitted for clarity. The thick shaded curves show peak T-X_{CO_2} conditions of fluid-rock systems metamorphosed at $P = 1$ kbar, $T = 350$–650 °C, and constant porosity (ϕ) with no flow. The relation between T and Z along the vertical axis is that specified by Eq. 1.

When the temperature of rock containing constant fluid-filled porosity and an isobaric univariant mineral assemblage increases, X_{CO_2} and y_{CO_2} of fluid change according to the curves in Figures 1 and 2. Equation 2 specifies reaction progress and hence mineralogical evolution of rock between an initial state at low temperature and a final state at high temperature. The equation describes an idealized situation, where any fluid volume produced by thermal expansion or reaction during transition from the initial to the final state is expelled to preserve a constant ϕ. Expelled fluid was not considered to interact further with rock. This might occur in nature if the fluid volume produced in excess of porosity escaped along fractures.

Porosity-distance maps. As an example of the computations, consider the Dol + Qtz rock with 12% porosity. The T-X_{CO_2} evolution of the fluid-rock system as it is heated to 650 °C is tracked by the appropriate shaded curve in Figure 1. At $T < 356$ °C, Dol + Qtz are stable. When rock is heated above 356 °C (the temperature at which Dol + Qtz + Tlc + Cal and fluid with $X_{CO_2} = 0.05$ are in equilibrium), Dol + Qtz react to Tlc + Cal:

$$3\ \text{Dol} + 4\ \text{Qtz} + H_2O = \text{Tlc} + 3\ \text{Cal} + 3CO_2. \quad (3)$$

The assemblage Dol + Qtz + Tlc + Cal is stable as the rock is heated between 356 and 422 °C ($Z = 876$–1279 m) because the calculated progress of Reaction 3, ξ_3, remains less than the maximum possible, 1.10175 mol/L.

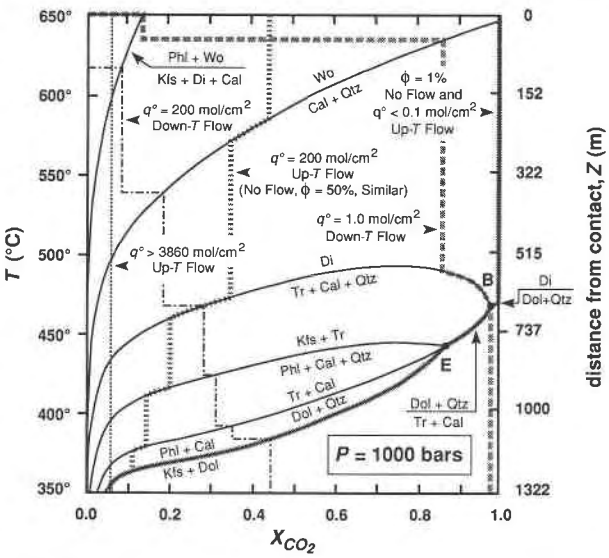

Fig. 2. Same as for Fig. 1 but for the model Kfs + Dol + Cal + Qtz rock and reactions involving Kfs, Dol, Phl, Cal, Qtz, Tr, Di, Wo, and CO_2-H_2O fluid. The thick shaded, dashed, and dotted curves show peak T-X_{CO_2} conditions of fluid-rock systems metamorphosed at P = 1 kbar and T = 350–650 °C with either no flow, up-temperature flow, or down-temperature flow, as indicated. In cases of flow, q^0 refers to the time-integrated fluid flux introduced at the inlet to the model aureole.

At 422 °C (Z = 876 m) the system encounters the isobaric invariant point A (Fig. 1), and ξ_3 = 0.886 mol/L. With the further addition of heat

$$0.685\ \text{Tlc} + 0.870\ \text{Cal} + 0.420\ \text{Qtz} = 0.395\ \text{Tr} + 0.080\ \text{Dol} + 0.710\text{CO}_2 + 0.290\text{H}_2\text{O} \quad (4)$$

(the stoichiometry was determined by the method of Rice and Ferry, 1982). The reaction proceeds until all Tlc is consumed, 0.511 mol Tr/L is produced, and 0.318 mol Qtz/L remains in the rock. With further increase in temperature, Dol + Qtz react to Tr + Cal:

$$5\ \text{Dol} + 8\ \text{Qtz} + \text{H}_2\text{O} = \text{Tr} + 3\ \text{Cal} + 7\text{CO}_2. \quad (5)$$

At T = 428 °C (Z = 849 m) pore fluid has the composition X_{CO_2} = 0.76 and ξ_5 = 0.0398, indicating that Qtz is exhausted. Dol + Tr + Cal + fluid are stable with continued increase in temperature until T = 537 °C (Z = 368 m). When rock is heated above 537 °C, Tr + Cal react to Di + Dol:

$$\text{Tr} + 3\ \text{Cal} = 4\ \text{Di} + \text{Dol} + \text{H}_2\text{O} + \text{CO}_2. \quad (6)$$

The assemblage Tr + Cal + Di + Dol is stable as the rock is heated between 537 and 547 °C (Z = 333–368 m) because ξ_6 remains less than the maximum possible, 0.550875 mol/L. At 547 °C (Z = 333 m) the system encounters the isobaric invariant point C (Fig. 1) and ξ_6 = 0.407 mol/L. With the addition of heat,

$$0.333\ \text{Tr} + 0.168\ \text{Dol} + 0.331\ \text{Cal} = 0.334\ \text{Fo} + 1.165\ \text{Di} + 0.667\text{CO}_2 + 0.333\text{H}_2\text{O}. \quad (7)$$

Reaction 7 proceeds at 547 °C until the remaining Tr is consumed and the rock contains 2.131 mol Di/L. With further increase in temperature, Dol + Di react to Fo + Cal:

$$\text{Di} + 3\ \text{Dol} = 2\ \text{Fo} + 4\ \text{Cal} + 2\text{CO}_2. \quad (8)$$

At T = 569 °C (Z = 254 m), pore fluid has the composition X_{CO_2} = 0.98 and ξ_8 = 2.131, indicating that Di is exhausted. The rock is composed of Fo + Dol + Cal, and no further reactions occur at $T \leq$ 650 °C ($Z \leq$ 254 m). The sequence of mineral reactions and the temperatures (Z values) at which they occur determined the sequence of stable mineral assemblages in Figure 3 for ϕ = 12%.

Repetition of the computation for other values of porosity maps out mineral assemblages in the other parts of Figure 3. Each field for an isobaric univariant assemblage may be contoured with the values of reaction progress computed from Equation 2 (e.g., the Dol + Qtz + Tlc + Cal field in Fig. 3; contours in the other univariant fields were omitted for clarity). Contours show how modes change spatially for a given ϕ, and may be used to distinguish whether or not fluid flowed in specific contact aureoles (as discussed below). The results of analogous computations starting with the Kfs + Dol + Cal + Qtz rock are summarized in Figure 4. For clarity, contours of the reaction progress are shown only for the Dol + Kfs + Phl + Cal + Qtz univariant field.

The final spatial distribution of mineral assemblages in the model aureole following peak metamorphism at constant porosity and no fluid flow corresponds to assemblages distributed along a horizontal transect through Figures 3 and 4 at the appropriate value of ϕ. Mineral assemblages in a real contact aureole where there was no fluid flow and constant porosity would correspond to those encountered along one or another of the horizontal lines.

Fluid flow in the direction of increasing temperature

General procedure. In the second model the rock is considered to be infiltrated by fluid flowing horizontally in the direction of increasing temperature. To satisfy assumptions of a steady-state temperature profile and local equilibrium, each protolith was first heated to temperatures defined by Equation 1 under conditions of no porosity or fluid flow and then allowed to equilibrate. Following heating and equilibration, the original Dol + Qtz rock was composed of Dol + Qtz at Z > 655 m, Di + Dol at Z = 250–655 m, and Fo + Dol + Cal at Z = 0–250 m. The original Kfs + Dol + Cal + Qtz rock was composed after heating and equilibration of Kfs + Dol + Cal + Qtz at Z > 655 m, Kfs + Di + Cal + Qtz at Z = 7–655 m, and Kfs + Wo + Di + Cal at Z = 0–7 m. The rock was then infiltrated by fluid, and the progress of mineral reactions was tracked as a function of time-integrated fluid flux (q) at each position Z. To facilitate comparison with the model for no flow, the composition of input fluid was set at X_{CO_2} = 0.05. After a given amount of flow, the final (peak) mineral assemblage was plotted on a diagram like Figure 5 or 6 at the appropriate values of Z and q. The calculation was repeated to cover a range of Z (0–1400 m) and q (0–10000 mol fluid/cm² rock).

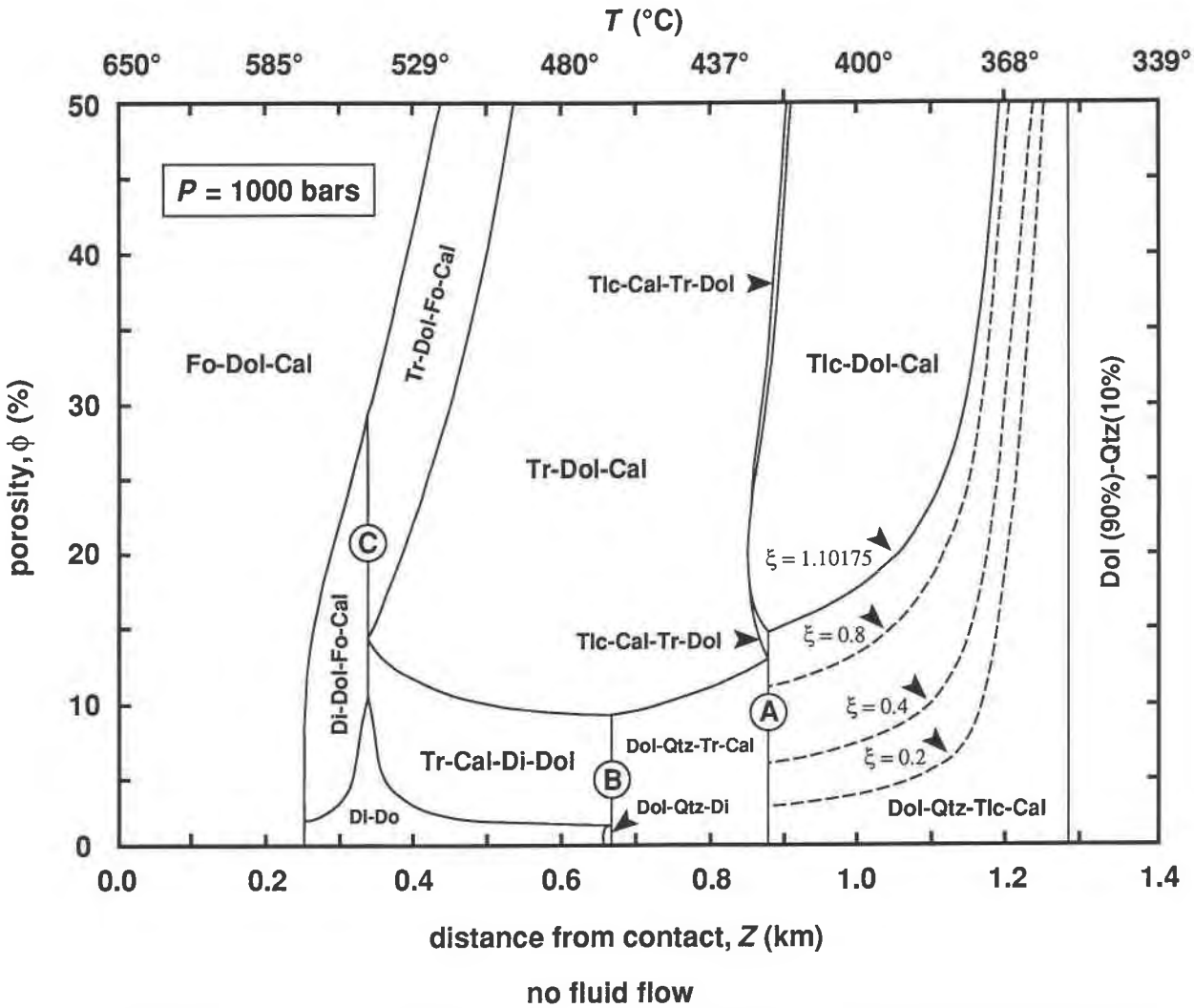

Fig. 3. Map of stable mineral assemblages in the model Dol + Qtz rock as a function of porosity and position along a distance coordinate where temperature varies according to Eq. 1. Porosity is filled with CO_2-H_2O fluid with initial composition $X_{CO_2} = 0.05$, and chemical effects of any fluid flow are neglected (see text for details). Percentages in the Dol + Qtz field refer to modal amounts of minerals in the protolith. Isobaric invariant assemblages occur along vertical line segments identified by letters that correspond to those in Fig. 1. The dashed curves are contours of the progress of Reaction 3 in the isobaric univariant assemblage Dol + Qtz + Tlc + Cal with units of moles per liter of rock. The top boundary of the Dol + Qtz + Tlc + Cal field is a contour of $\xi = 1.10175$ mol/L.

Progress of a mineral-fluid reaction is quantitatively related to q at most spatial points by

$$q = \frac{\xi[\nu_{CO_2} - X_{CO_2}(\nu_{CO_2} + \nu_{H_2O})]}{(\partial X_{CO_2}/\partial T)_P(dT/dz)} \quad (9)$$

(Baumgartner and Ferry, 1991). A $(\partial X_{CO_2}/\partial P)_T(dP/dz)$ term, which is very small because flow is assumed to be horizontal, was ignored. In Equation 9 it was assumed that the rock had a small porosity (the exact value is immaterial) and that mass transfer by diffusion and dispersion was negligible; the latter assumption is plausible given the temporal and spatial scale over which mineral assemblages develop in contact aureoles. The distance coordinate (z) of Equation 9 is antiparallel to the distance coordinate Z of the temperature profile (Eq. 1). Values of dT/dz, the horizontal temperature gradient, were obtained by differentiating the negative of Equation 1 with respect to Z; values of $(\partial X_{CO_2}/\partial T)_T$ are the inverses of slopes of T-X_{CO_2} curves in Figures 1 and 2.

Flux-distance maps. Most phase fields in Figures 5 and 6 were located by computing the value of q for points that correspond to a given X_{CO_2} along the boundaries of each isobaric univariant field. As an example, consider the Dol + Qtz rock and $X_{CO_2} = 0.14$. The instant that fluid infiltrates the model aureole, Reaction 3 initiates at $Z = 1279$ m (corresponding to the temperature at which Dol + Qtz + Tlc + Cal are in equilibrium with the fluid of $X_{CO_2} = 0.05$) and at points farther downstream at higher values of X_{CO_2}. With continued infiltration, Reaction 3

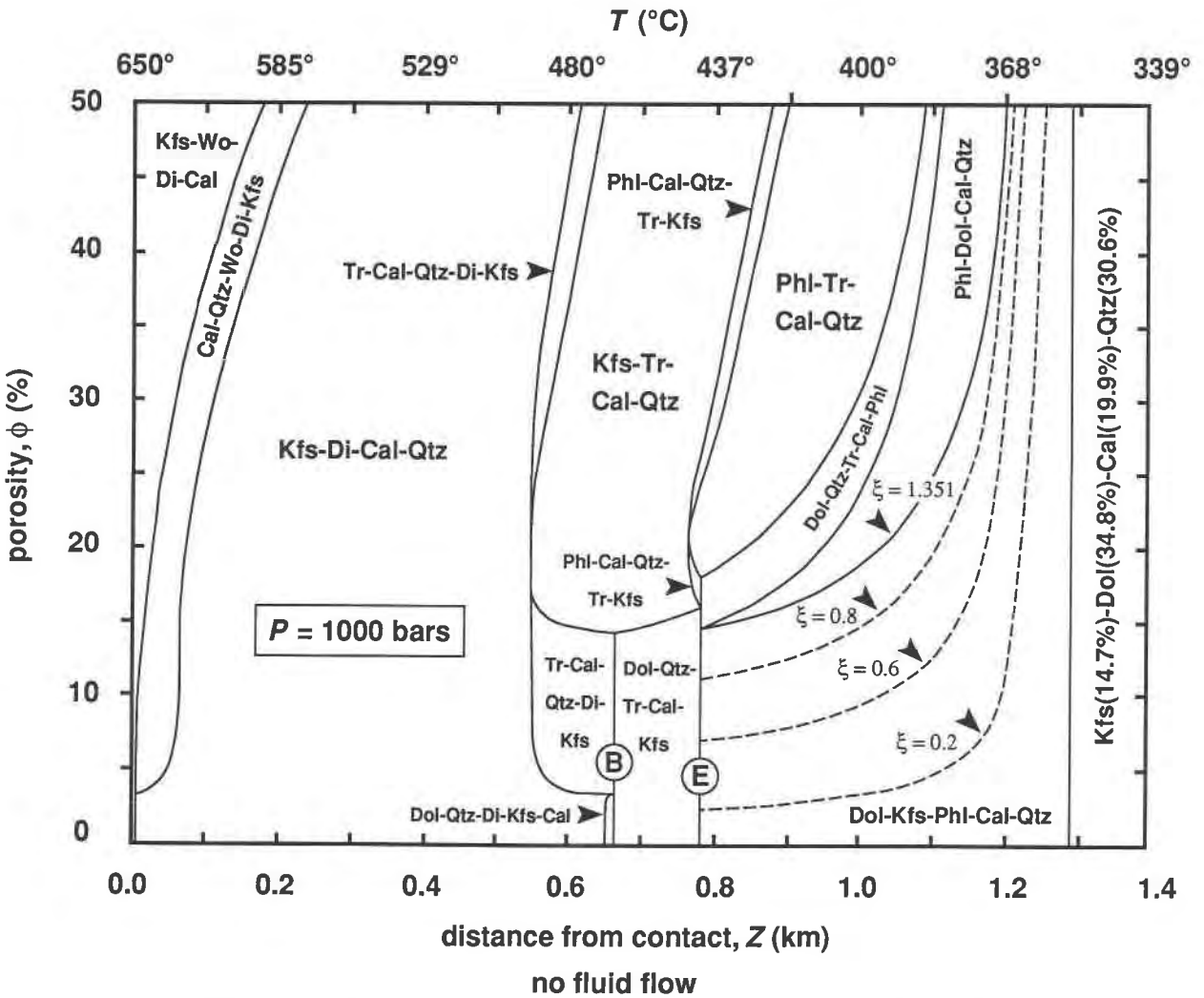

Fig. 4. Same as for Fig. 3 but for the model Kfs + Dol + Cal + Qtz rock. The letters refer to isobaric invariant points in Fig. 2. The dashed lines are contours of the progress of the reaction 3 Dol + Kfs + H_2O = Phl + 3 Cal + $3CO_2$ with units of moles per liter of rock.

proceeds where X_{CO_2} = 0.14 (T = 369 °C, Z = 1188 m) until Qtz is exhausted (ξ_3 = 1.10175 mol/L). The value of q calculated from Equation 9 for ξ_3 = 1.10175 mol/L at Z = 1188 m is 136.5 mol/cm². The result gives a q-Z point on the boundary between the Dol + Qtz + Tlc + Cal and Tlc + Dol + Cal fields on Figure 5.

The instant quartz is exhausted at Z = 1188 m, the reaction

$$2\ \text{Tlc} + 3\ \text{Cal} = \text{Tr} + \text{Dol} + CO_2 + H_2O \quad (10)$$

initiates at the point downstream where Tlc + Cal + Tr + Dol and fluid with X_{CO_2} = 0.14 are in equilibrium (T = 417 °C, Z = 906 m). The time-integrated flux at 906 m when Tr first appears therefore is the sum of 136.5 mol/cm² and the amount of fluid produced earlier in the interval Z = 906–1188 m during the conversion of Dol + Qtz to Tlc + Cal by Reaction 3 (62.1 mol/cm²). The sum, 198.6 mol/cm², provides one point on the boundary between the Tlc + Dol + Cal and Tlc + Cal + Tr + Dol fields. With continued infiltration, Reaction 10 proceeds until Tlc is exhausted (ξ_{10} = 0.550875 mol/L). The value of q calculated from Equation 9 for ξ_{10} = 0.550875 mol/L at Z = 906 m is 14.4 mol/cm². The sum, 198.6 + 14.4 = 213.0 mol/cm², provides a q-Z point on the boundary between the Tlc + Cal + Tr + Dol and Tr + Dol + Cal fields.

The instant talc is exhausted at Z = 906 m, the reaction

$$\text{Tr} + 11\ \text{Dol} = 8\ \text{Fo} + 13\ \text{Cal} + 9CO_2 + H_2O \quad (11)$$

initiates downstream at the point where Tr + Dol + Fo + Cal and fluid with X_{CO_2} = 0.14 are in equilibrium (T = 494 °C, Z = 541 m). The time-integrated flux at 541 m when Fo first appears therefore is the sum of 213.0 mol/cm² and the amount of fluid produced earlier in the interval Z = 541–906 m during the conversion of Dol + Qtz (Z = 655–906 m) or Di + Dol (Z = 541–655 m) to Tr + Dol + Cal by Reactions 3, 6, and 10 (70.4 mol/

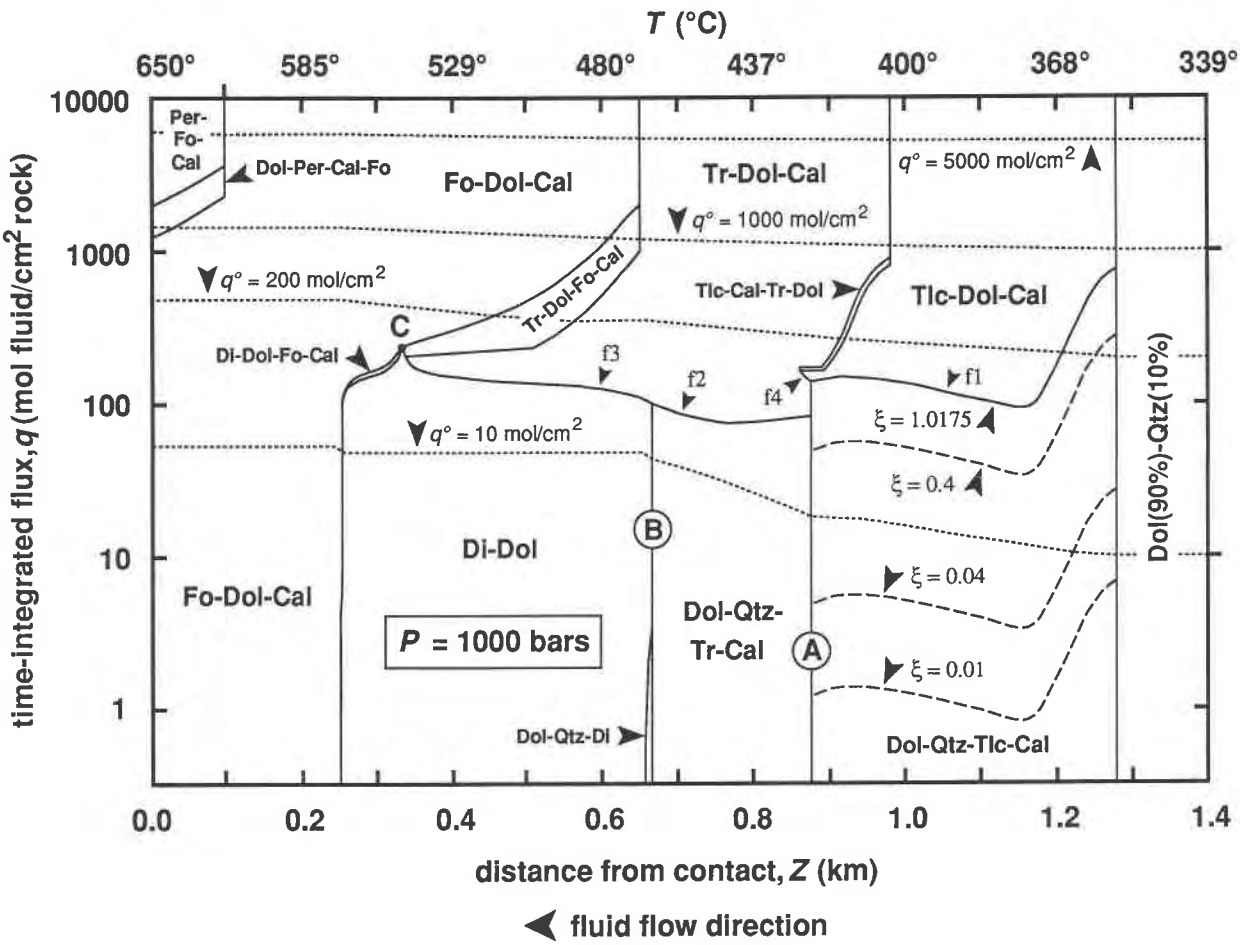

Fig. 5. Map of stable mineral assemblages in the model Dol + Qtz rock as a function of time-integrated fluid flux and position along a distance coordinate, where temperature varies according to Eq. 1. Input fluid is a CO_2-H_2O solution with X_{CO_2} = 0.05, and flow is in the direction of increasing temperature (see text for details). Percentages in the Dol + Qtz field refer to modal amounts of minerals in the protolith. Isobaric invariant assemblages occur at points or along vertical line segments identified by letters that correspond to those in Fig. 1. Dashed curves are contours of the progress of Reaction 3 in the isobaric univariant assemblage Dol + Qtz + Tlc + Cal with units of moles per liter of rock. The top boundary of the Dol + Qtz + Tlc + Cal field is a contour of ξ = 1.10175 mol/L. Dotted curves illustrate the increase in time-integrated flux from input values of q^0 = 10, 200, 1000, and 5000 mol/cm² at $Z > 1400$ m due to production of CO_2 and H_2O by devolatilization reactions along the flow path. Curves marked f1–f4 are reaction fronts described in the text.

cm²). The sum, 283.4 mol/cm², provides one point on the boundary between the Tr + Dol + Cal and Tr + Dol + Fo + Cal fields. Reaction 11 proceeds until Tr is exhausted (ξ_{11} = 0.550 875 mol/L). The value of q calculated from Equation 9 for ξ_{11} = 0.550 875 mol/L at Z = 541 m is 343.1 mol/cm². The sum, 283.4 + 343.1 = 626.5 mol/cm², gives a q-Z point on the boundary between the Tr + Dol + Fo + Cal and Fo + Dol + Cal fields.

Repetition of these or similar calculations for other values of X_{CO_2} determines the boundaries of most of the isobaric univariant fields. Parts of several phase fields on Figure 5, however, were located using other equations. Reaction 3 first goes to completion at Z = 1183 m because of the inflection point on its T-X_{CO_2} curve. A Tlc + Dol + Cal band centered on Z = 1183 m then develops bounded by Dol + Qtz + Tlc + Cal at both greater and smaller Z. This corresponds to the trough on the boundary between the Dol + Qtz + Tlc + Cal and Tlc + Dol + Cal fields in Figure 5. Reaction 3 at the inner (low-Z) boundary is driven by infiltration of fluid that departs from equilibrium with Dol + Qtz + Tlc + Cal by a finite amount, and Equation 9 is inapplicable. Let position, fluid composition, and time-integrated flux at the outer (high Z) boundary be Z_0, X_0, and q_0, respectively (q_0 was calculated from Equation 9); equivalent variables at the inner boundary are Z_1, X_1, and q_1. The composition of the infiltrating fluid at Z_1 therefore is X_0. Z_1 is that position, computed by trial and error, where

$$[(X_0)(q_0) + n_{CO_2}]/[q_0 + n_{CO_2} - n_{H_2O}] = X_1 \qquad (12)$$

with n_{CO_2} and n_{H_2O} the moles of CO_2 produced and moles of H_2O consumed per square centimeter of rock by Re-

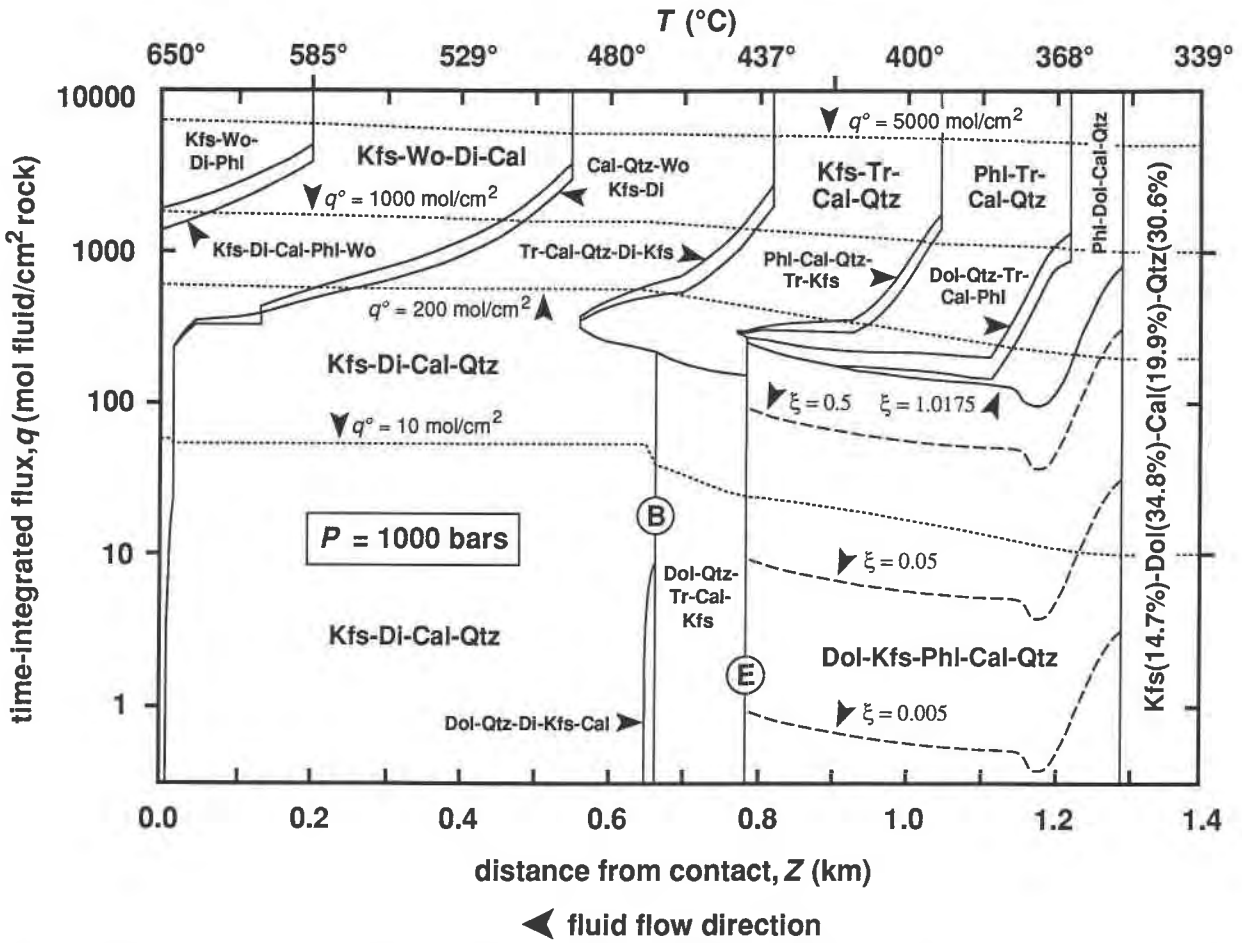

Fig. 6. Same as for Fig. 5 but for the model Kfs + Dol + Cal + Qtz rock. The letters refer to isobaric invariant points in Fig. 2. The dashed lines are contours of the progress of the reaction, 3 Dol + Kfs + H_2O = Phl + 3 Cal + $3CO_2$ with units of moles per liter of rock.

action 3 in the interval between Z_0 and Z_1 since the time Qtz was first exhausted at 1183 m. The value of q_1 at Z_1 is $q_0 + n_{CO_2} - n_{H_2O}$. The boundary between the Dol + Qtz + Tlc + Cal and Tlc + Dol + Cal fields at Z = 876–1183 m was computed from Equation 12 (f1, Fig. 5). The boundary between the Dol + Qtz + Tr + Cal and Tr + Dol + Cal fields at Z = 663–710 m was calculated analogously (f2, Fig. 5).

After fluid flow destroys the isobaric invariant assemblage Dol + Qtz + Tr + Di + Cal at Z = 663 m (when q = 100 mol/cm²), further infiltration converts Di + Dol to Tr + Dol + Cal in the interval Z = 333–663 m at a sharp front by Reaction 6. At the same time a boundary between the assemblages Tr + Dol + Cal and Dol + Qtz + Tr + Cal exists at Z > 710 m. Let position, fluid composition, and time-integrated flux at the reaction front be Z_3, X_3, and q_3, respectively. Equivalent variables at the boundary between assemblages Tr + Dol + Cal and Dol + Qtz + Tr + Cal are Z_2, X_2, and q_2 (all calculated as described above). The infiltrating fluid at the reaction front has composition X_2. After infiltration at 663 m of a first tiny increment of input fluid, Δq, Di + Dol is converted to Tr + Dol + Cal over a small distance interval, ΔZ. The size of ΔZ is calculated by trial and error so that

$$\Delta q = (\xi_{max})(\Delta Z)[\nu_{CO_2} - X_3(\nu_{CO_2} + \nu_{H_2O})]/(X_3 - X_2) \quad (13)$$

where ξ_{max} is the maximum progress of Reaction 6 possible in the protolith (0.550 875 mol/L), ν_{CO_2} and ν_{H_2O} are the stoichiometric coefficients of CO_2 and H_2O in the reaction, and X_3 is defined by equilibrium of fluid with Di + Dol + Tr + Cal. The reaction front (and boundary between the Di + Dol and Tr + Dol + Cal fields) is then located at $Z_3 = 663 - \Delta Z$ and q_3 is the sum of q_2, $[(\Delta Z)(\xi_{max})(\nu_{CO_2} + \nu_{H_2O})]$, and the moles of volatiles released during the prior conversion of Dol + Qtz to Tr + Dol + Cal in the interval Z_2 to 663 m. The rest of the boundary between the Di + Dol and Tr + Dol + Cal fields at Z > 333 m was located by repeating the calculation for additional increments of input fluid (f3, Fig. 5). The boundary between the Tr + Dol + Cal and Tlc + Dol + Cal fields at Z = 863–876 m was calculated anal-

ogously (f4, Fig. 5). Input values of Δq were varied by a factor of ten to verify that calculated positions of the phase fields were stable with respect to the size of Δq. The results of all calculations for fluid flow in the direction of increasing temperature through the initial Dol + Qtz rock are summarized in Figure 5.

The results of analogous computations starting with the Kfs + Dol + Cal + Qtz rock are summarized in Figure 6. The positions of most phase fields were computed from Equation 9. The boundaries between the Dol + Kfs + Phl + Cal + Qtz and Phl + Dol + Cal + Qtz fields at Z = 785–1180 m and between the Dol + Qtz + Tr + Cal + Kfs and Kfs + Tr + Cal + Qtz fields at Z = 663–710 m were calculated using Equation 12. The boundaries between the Kfs + Di + Cal + Qtz and Kfs + Tr + Cal + Qtz fields at Z = 563–663 m and between the Kfs + Tr + Cal + Qtz and Phl + Tr + Cal + Qtz fields at Z = 775–785 m were located using Equation 13. Fields for each isobarically univariant assemblage may be contoured with values of reaction progress computed from Equation 9 (e.g., the Dol + Qtz + Tlc + Cal field in Fig. 5 and the Dol + Kfs + Phl + Cal + Qtz field in Fig. 6). The contours in the other univariant fields were omitted for clarity.

Time-integrated flux, q, increases along the flow path because of internal production of volatiles by reactions, and the increase may be computed from Equation 13 of Baumgartner and Ferry (1991). Results for a time-integrated input fluid flux, q^0, of 10, 200, 1000, and 5000 mol/cm^2 are shown by dotted curves in Figures 5 and 6. If there were an influx of 10 mol fluid/cm^2 rock into the low-temperature end of the model aureole and up-temperature flow, the bottom dotted curve illustrates the time-integrated flux that would have passed by each point downstream by the conclusion of the metamorphic event. The final spatial distribution of mineral assemblages corresponds to that encountered along the curve for q^0 = 10 mol/cm^2 through Figures 5 and 6. For contact metamorphism involving other values of q^0 and fluid flow in the direction of increasing temperature, predicted mineral assemblages and their positions along the distance coordinate would be read off equivalent curves for the appropriate value of time-integrated input fluid flux, q^0. Mineral assemblages exposed in a real contact aureole where fluid flowed horizontally up-temperature would correspond to those along one or another of such curves.

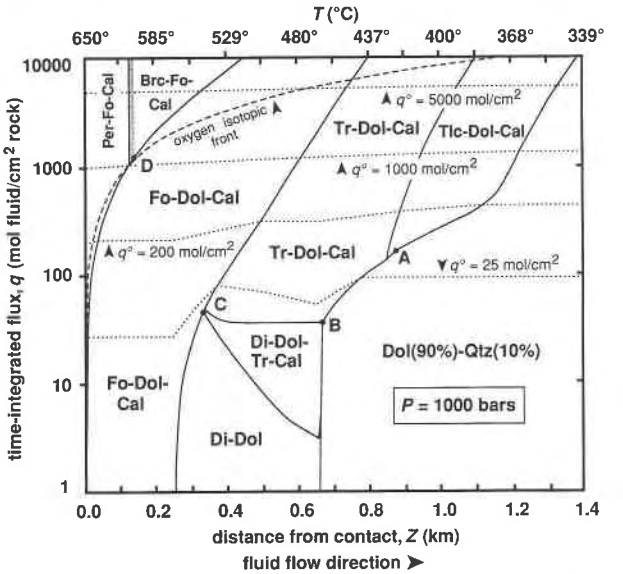

Fig. 7. Map of stable mineral assemblages in the model Dol + Qtz rock as a function of time-integrated fluid flux and position along a distance coordinate, where temperature varies according to Eq. 1. Input fluid is pure H_2O, and flow is in the direction of decreasing temperature. Percentages in the Dol + Qtz field refer to modal amounts of minerals in protolith. Isobaric invariant assemblages occur at points identified by letters that correspond to those in Fig. 1. The dotted curves illustrate the change in time-integrated flux from input values of q^0 = 25, 200, 1000, and 5000 mol/cm^2 at Z = 0 due to production and consumption of CO_2 and H_2O by mineral-fluid reactions along the flow path. The shaded area identifies the region where peak brucite occurs as a replacement of earlier periclase; brucite is primary elsewhere in its stability field. The dashed line shows the position of an O isotope alteration front that develops if the input fluid has isotopic composition different from that in equilibrium with metacarbonate rock. See text for details.

Fluid flow in the direction of decreasing temperature

General procedure. In the third model a rock is considered to be infiltrated by fluid flowing horizontally in the direction of decreasing temperature. Because the likely source of input fluid would be the igneous intrusion, the fluid was considered pure H_2O. The two model rocks initially have the same mineral assemblage as at the start of calculations for the up-temperature flow model. When the model aureole is infiltrated by the H_2O fluid, the progress of mineral reactions is tracked at each position Z as a function of time-integrated fluid flux. Calculations cover Z = 0–1400 m and q = 0–10000 mol/cm^2. The results map out the stability fields for mineral assemblages as a function of the two variables (Figs. 7 and 8).

Flux-distance maps. Figures 7 and 8 were constructed by calculating the innermost (low-Z) boundaries between phase fields and proceeding outward. Consider the initial Dol + Qtz rock and the boundaries between the Per + Fo + Cal and Fo + Dol + Cal fields and between the Fo + Dol + Cal and Di + Dol fields. The boundary between the Per + Fo + Cal and Fo + Dol + Cal fields corresponds to a sharp front along which reactants and products of

$$\text{Dol} = \text{Per} + \text{Cal} + \text{CO}_2 \qquad (14)$$

coexist (see Ferry, 1991). For the first increment of input fluid, Δq, the corresponding increment of distance, ΔZ, that the front moves away from the contact at Z = 0 is specified by Equation 13, with $\nu_{CO_2} = 1$, $\nu_{H_2O} = 0$, $X_2 = 0$, ξ_{max} = 5.179 mol/L, and X_3 is the composition of fluid in equilibrium with Dol + Per + Cal at the midpoint of ΔZ. In practice, a small value of ΔZ is chosen and the

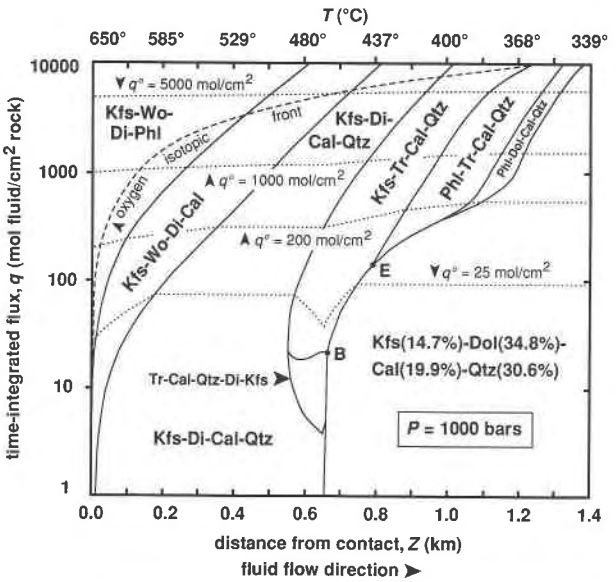

Fig. 8. Same as for Fig. 7 but for the model Kfs + Dol + Cal + Qtz rock. The letters refer to isobaric invariant points in Fig. 2.

associated value of Δq is computed from Equation 13. The value of time-integrated flux used to plot the boundary on Figure 7 is Δq plus the moles of CO_2 produced by Reaction 14 in the interval ΔZ. The calculation is repeated for additional increments of input fluid, and the boundary moves from $Z = 0$ at $q = 0$ to $Z = 129$ m at $q = 1090$ mol/cm², where Reaction 14 involving Per is replaced with one involving Brc. The position of the boundary calculated from Equation 13 is identical to its position independently calculated from Equation 15 of Ferry (1991).

The computation of the position of the boundary between the Per + Fo + Cal and Fo + Dol + Cal fields predicts the amount and composition of the first increment of fluid after it passes the reaction front. These values then serve as input for calculating the position of the next reaction front downstream, corresponding to the boundary between the Fo + Dol + Cal and Di + Dol phase fields and to Reaction 8. After flow commences, the front moves from its initial position at 250 m outward an increment of distance ΔZ. The value of ΔZ is computed from Equation 13 with $\nu_{CO_2} = 2$, $\nu_{H_2O} = 0$, $\xi_{max} = 2.2035$ mol/L, X_3 is the composition of fluid in equilibrium with Di + Dol + Fo + Cal at the midpoint of the distance interval, and X_2 and Δq are the output from calculating the position of the boundary between the Per + Fo + Cal and Fo + Dol + Cal fields. The value of time-integrated flux used to plot the front on Figure 7 is Δq plus the moles of CO_2 produced by Reaction 8 in the interval ΔZ. The calculation is repeated for additional increments of input fluid, and the boundary moves from $Z = 250$ m at $q = 0$ to $Z = 333$ m at $q = 46$ mol/cm², where Reaction 8 is replaced with other reactions involving Tr.

The positions of all boundaries but the upper limit of the Di + Dol + Tr + Cal field on Figure 7 were calculated in an analogous fashion. Fluid downstream from the reaction front corresponding to the boundary between the Fo + Dol + Cal and Di + Dol fields hydrates and carbonates an initial Di + Dol assemblage to Tr + Dol + Cal by means of Reaction 6. Reaction 6 occurs not at a sharp front but continuously in the interval $Z = 333$–663 m. Completion of the reaction, which corresponds to the upper boundary of the Di + Dol + Tr + Cal field in Figure 7, therefore was calculated using Equation 9. The results of all calculations for fluid flow in the direction of decreasing temperature through the initial Dol + Qtz rock are summarized in Figure 7. Not obvious from the diagram are an infinitesimally thin layer of Per + Fo + Cal that separates the Brc + Fo + Cal and Fo + Dol + Cal fields in the interval $q = 1090$–1260 mol/cm², a thin layer of Tr + Dol + Cal that separates the Tlc + Dol + Cal + and Dol + Qtz fields at $q = 140$–165 mol/cm², and a thin layer of Tr + Dol + Cal that separates the Fo + Dol + Cal and Di + Dol + Tr + Cal fields at 46–50 mol/cm². The thin layers develop when a faster-moving reaction front initiated upstream overtakes with a slower-moving front downstream.

The results of analogous computations starting with the Kfs + Dol + Cal + Qtz rock are summarized in Figure 8. The boundaries of all phase fields were computed with Equation 13, except for part of the upper boundary of the Tr + Cal + Qtz + Di + Kfs field, which was computed from Equation 9. Not obvious from the diagram are an infinitesimally thin layer of Phl + Dol + Cal + Qtz, which separates the Phl + Tr + Cal + Qtz and Kfs + Dol + Cal + Qtz fields in the interval $q = 140$–375 mol/cm², and thin layers of Phl + Tr + Cal + Qtz and Kfs + Tr + Cal + Qtz, which separate the Kfs + Tr + Cal + Qtz and Kfs + Dol + Cal + Qtz fields at $q = 120$–140 mol/cm².

Time-integrated flux, q, changes along the flow path because of the internal production and consumption of volatiles by reactions. The changes can be computed at each point Z by adding the time-integrated input fluid flux at the high-temperature inlet of the aureole to the sum of volatiles produced or consumed by reactions between Z and the contact. Results for a time-integrated input fluid flux, q^0, of 25, 200, 1000, and 5000 mol/cm² are shown by the dotted curves in Figures 7 and 8. Portions of the curves where q decreases with increasing Z correspond to regions where CO_2 and H_2O in fluid are consumed in the production of Tr + Cal ± Qtz from Di ± Dol. The dotted curves have the same significance as those in Figures 5 and 6. The final distribution of mineral assemblages produced by a time-integrated input fluid flux of 25 mol/cm² and down-temperature flow, for example, corresponds to assemblages encountered along the bottom dotted curve in Figures 7 and 8. For metamorphism involving other values of q^0 and fluid flow in the direction of decreasing temperature, predicted mineral assemblages and their positions along the distance coordinate would be read off equivalent curves for the appro-

priate value of time-integrated input fluid flux. Mineral assemblages in a real contact aureole where fluid flowed horizontally down-temperature would correspond to those along one or another of such curves.

Discussion

The effect of input parameters and assumptions on calculated results. All results were calculated with respect to a single pressure, a single relation between temperature and distance within the model contact aureole, and two specific rock compositions. Although it is beyond the scope of the paper to explore quantitatively the effect of varying these input parameters, the effects may be evaluated qualitatively. Because the temperature of devolatilization equilibria typically increases with increasing pressure, the phase fields in the ϕ-Z and q-Z maps will move to lower values of Z if $P > 1$ kbar and to greater values of Z if $P < 1$ kbar. If the temperature profile were steeper than that in Equation 1 but the temperature at the contact were the same, the fields in the ϕ-Z and q-Z diagrams would move to lower values of Z; a gentler profile would have the opposite effect. A higher temperature at the contact would expand fields for high-T and low-X_{CO_2} assemblages like Per + Fo + Cal and Kfs + Wo + Di + Phl; a lower contact temperature would have the opposite effect. If the protoliths had a higher silicate-carbonate ratio, phase fields in the ϕ-Z and q-Z diagrams would shift upward because greater porosity or greater time-integrated flux would be required to drive reactions to completion. Smaller silicate-carbonate ratios would have the opposite effect.

If the protoliths in the flow models contained a small porosity (<1%) initially filled with fluid of the composition $X_{CO_2} = 0.05$, the mineral assemblages in the aureoles, following heating to peak temperatures but prior to flow, would be those in Figures 3 and 4 for $\phi < 1\%$. These assemblages and their positions are identical to those predicted by the up-temperature flow model for $q < \approx 1$ mol/cm^2. In the case of up-temperature flow, therefore, it effectively makes no difference to the final results whether the protolith initially contained no porosity or a small porosity (in detail, the phase fields in Figs. 5 and 6 would be shifted downward by ≈ 1 mol/cm^2 or less if the protolith contained a porosity $\leq 1\%$). If the protolith initially contained <1% porosity, down-temperature flow with $q \approx 1$ mol/cm^2 converts the initial mineral assemblage prior to flow to that depicted along the bottom of Figures 7 and 8. For down-temperature flow it effectively makes no difference as well to final results at $q > 1$ mol/cm^2 whether the protolith initially contains no porosity or a small porosity (in detail, the phase fields in Figs. 7 and 8 would be shifted upward ≈ 1 mol/cm^2 or less if the protolith contained a porosity $\leq 1\%$).

Geometry of fluid flow. A fundamental question in the mineralogic evolution of contact metamorphosed siliceous dolomitic limestones is whether fluid flow was horizontal and up-temperature, was horizontal and down-temperature, had some other geometry, or was absent. There are many ways in which the question may be answered for specific aureoles. Simply the occurrence of a particular mineral may be informative. The presence of periclase in siliceous dolomites rules out metamorphism without fluid flow, and the presence of primary brucite rules out both lack of flow and flow in the direction of increasing temperature.

The distribution of isobaric invariant and univariant assemblages produced during fluid flow is different depending on whether flow is up- or down-temperature ($dT/dz > 0$ and $dT/dz < 0$, respectively). In both cases, when $(\partial X_{CO_2}/\partial T)_P$ and (dT/dz) have opposite algebraic signs, isobaric univariant assemblages develop only at sharp reaction fronts (Figs. 5–8). When $(\partial X_{CO_2}/\partial T)_P$ and (dT/dz) have the same sign, isobaric univariant assemblages are dispersed for a significant distance along the flow path (provided q is not too large). Widespread distribution in the field of univariant assemblages like Dol + Qtz + Tlc + Cal and Dol + Qtz + Tr + Cal that define positive $(\partial X_{CO_2}/\partial T)_P$ and restricted occurrence of assemblages like Tr + Cal + Di + Dol that define negative $(\partial X_{CO_2}/\partial T)_P$ therefore record up-temperature flow. Conversely, restricted occurrence of assemblages like Dol + Qtz + Tlc + Cal and Dol + Qtz + Tr + Cal and widespread distribution of assemblages like Tr + Cal + Di + Dol record down-temperature flow. When fluid flows in the direction of increasing temperature, some isobaric invariant assemblages are stable over a range of q, whereas invariant assemblages are stable at a single value of q when flow is in the direction of decreasing temperature (Figs. 5–8). The occurrence of an invariant assemblage like Dol + Qtz + Tlc + Cal + Tr in an aureole indicates up-temperature flow, whereas the absence of invariant assemblages is consistent with down-temperature flow. The spatial distribution of isobaric univariant and invariant assemblages is usually sufficient to distinguish between up-temperature and down-temperature flow.

It is more difficult to distinguish up-temperature flow from no flow because in both cases isobaric invariant and widespread univariant assemblages are expected (Figs. 3–6). If the time-integrated flux is large, the occurrence of periclase unambiguously indicates up-temperature flow. A second way to distinguish no flow from up-temperature flow is the examination of the relation between reaction progress (measured from the modal abundance of mineral products) and distance in the aureole. The difference in the shape of the contours of reaction progress in the univariant fields of Figures 3–6 indicates that reaction progress changes differently with distance depending on whether the pore fluid flows or not. Figure 9 shows explicitly how reaction progress in the assemblage Dol + Qtz + Tlc + Cal changes with distance for the cases of no flow and up-temperature flow. If there is no flow, reaction progress increases monotonically from a value of zero at the outer limit of the univariant field to a maximum value at the inner limit. If up-temperature flow occurs, reaction progress assumes a finite value at the outer limit of the univariant field, increases to a maximum in the middle of the field, and then decreases toward the

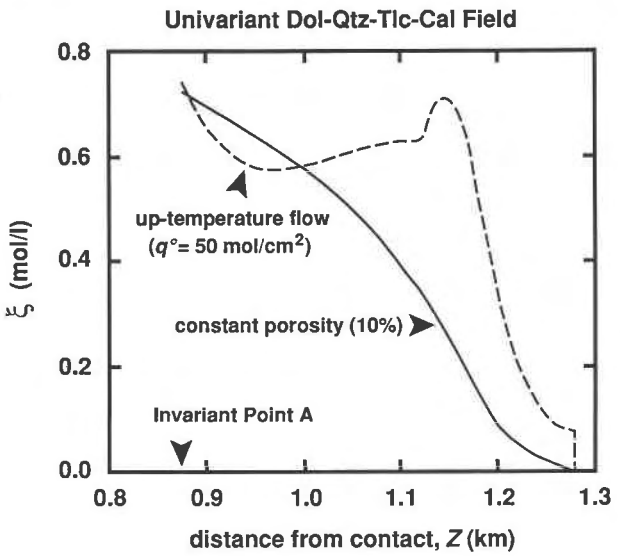

Fig. 9. Progress of Reaction 3 in the model Dol + Qtz rock as a function of distance between $Z = 1279$ m (outermost position of reaction), and $Z = 876$ m (position of isobaric invariant point A, Fig. 1, and the innermost position of reaction). The solid curve is the model for constant 10% porosity filled with CO_2-H_2O fluid, initial $X_{CO_2} = 0.05$, and no fluid flow; the dashed curve is the model for fluid flow in the direction of increasing temperature and an input of $q^0 = 50$ mol/cm² fluid with $X_{CO_2} = 0.05$ at $Z > 1279$ m. The differences between the curves allow discrimination between conditions of no flow and up-temperature flow from the measurement of ξ-Z relations in specific contact aureoles.

inner limit. Another way to evaluate whether no flow or up-temperature flow occurred is to assess the plausibility that $\phi > 10\%$, as is implied if many commonly observed mineral assemblages develop in the absence of fluid flow (Figs. 3 and 4). The likelihood of synmetamorphic porosity of >10% seems small for two reasons. First, large porosity is not obliterated by low-grade metamorphism or postmetamorphic processes because it is occasionally preserved in the low-grade portions of some aureoles (e.g., Bucher-Nurminen, 1982). The general observation that ϕ is rarely >1% in low-grade parts of contact aureoles therefore suggests that values as high as 10% are atypical. Second, at the elevated temperatures of the inner parts of contact aureoles, porosities of >10% are probably mechanically unstable and will be eliminated by compaction on a time scale of 200 yr or less (Bickle and Baker, 1990). Even if $\phi > 10\%$ existed initially or somehow developed transiently during metamorphism, it is unlikely that it could be maintained at high temperatures.

Although model calculations do not explicitly include vertical fluid flow, results suggest a way that it could be identified. Periclase only develops under conditions of fluid flow. The mineral is often closely associated spatially with F metasomatism and the development of calc-silicate skarns (e.g., Moore and Kerrick, 1976; Bowman and Essene, 1982; Holness, 1990, 1992). Although periclase in principle may develop from up-temperature flow at large values of time-integrated flux, the field observations are more consistent with formation by flow of magmatic fluids in the direction of decreasing temperature near the contact. The flow could be horizontal or vertical. The O isotope composition of marine carbonates differs significantly from that of typical magmatic fluids (e.g., Taylor, 1977). Horizontal, down-temperature flow of magmatic fluid into siliceous dolomitic limestone therefore should cause an associated O isotope alteration front to develop whose position, shown by the dashed curve in Figure 7, may be calculated from Equation 9 of Dipple and Ferry (1992). If periclase is produced by horizontal flow, the distance between the periclase isograd and the contact records the time-integrated flux, and an associated O isotope alteration front should exist at or near the predicted position. If the isotope front is absent or significantly deviates from the predicted position, vertical flow is indicated. Spatial relations between the outer limit of the assemblage Kfs + Wo + Di + Phl and an O isotope alternation front likewise would record whether fluid flow was horizontal or vertical in the metamorphosed equivalents to the Kfs + Dol + Cal + Qtz rock (Fig. 8).

Amount of fluid. Once it is established that there was no flow, up-temperature horizontal flow, or down-temperature horizontal flow, observed mineral assemblages and their spatial distributions in aureoles constrain the amount of fluid involved in contact metamorphism. The occurrence of an individual mineral may set a limit (diopside is possible in the model siliceous dolomite only at $\phi < 29\%$ for no flow, $q < 235$ mol/cm² for up-temperature flow, and $q < 50$ mol/cm² for down-temperature flow). With few exceptions, mineral assemblages of all variances provide constraints. The isobaric invariant assemblage Dol + Qtz + Tlc + Tr + Cal is stable at $\phi < 14\%$ for no flow, $q < 135$ mol/cm² for up-temperature flow, and $q = 165$ mol/cm² for down-temperature flow; the univariant assemblage Dol + Qtz + Tr + Cal at $\phi < 12\%$ for no flow, $q < 100$ mol/cm² for up-temperature flow, and $q = 37$–165 mol/cm² for down-temperature flow; and the divariant assemblage Tlc + Dol + Cal at $\phi > 14\%$ for no flow, $q > 91$ mol/cm² for up-temperature flow, and $q > 140$ mol/cm² for down-temperature flow (Figs. 3–7). The limits on ϕ and q provided by all assemblages in Figures 3–8 are summarized in Tables 1 and 2.

As a corollary, the nature of isograd reactions in specific contact aureoles constrains ϕ and q. If the forsterite isograd developed by Reaction 8, $\phi < 14\%$ for no flow, $q < 200$ mol/cm² for up-temperature flow, and $q < 46$ mol/cm² for down-temperature flow; if the isograd developed by Reaction 11, $\phi > 14\%$ for no flow, $q > 200$ mol/cm² for up-temperature flow, and $q > 46$ mol/cm² for down-temperature flow.

The most accurate estimates of fluid amount can be made from the measured distance of boundaries between phase fields and the contact. For example, the distance of the boundary between the Tr + Dol + Cal and Tr + Cal + Di + Dol fields (the diopside isograd) from the contact

TABLE 1. Observed mineral assemblages developed in contact metamorphosed siliceous dolomite, model rock composition SD, and limits on their conditions of formation

Assemblage	Limits*			Observed occurrences**			
	Constant ϕ	Up-T flow	Down-T flow	Beinn an Dubhaich	Alta	Elkhorn	Kasu-gamura
Dol + Qtz + Tlc + Tr + Cal	<14%	<135	165	x	?	o	x
Dol + Qtz + Tr + Di + Cal	<9%	<100	37	o	o	o	x
Dol + Tr + Fo + Di + Cal	11–29%	235	46	x	o	o	x
Per + Brc + Dol + Cal + Fo	impossible	impossible	1260	o	o	o	o
Dol + Qtz + Tlc + Cal	no limit	WD: <760 ND: >760	>165	WD	WD	o	WD
Dol + Qtz + Tr + Cal	<12%	<100	37–165	x	?	o	WD
Tlc + Cal + Tr + Dol	>12%	WD: 170–920 ND: 135–170; >920	>165	x	?	o	WD
Di + Dol + Tr + Cal	2–14%	100–235	3.2–50	o	o	o	x
Di + Dol + Fo + Cal	WD: 2–29% ND: <2%	WD: 135–240 ND: <135	<46	o	o	o	x
Tr + Dol + Fo + Cal	>14%	WD: 200–2050 ND: >2050	>46	WD	x	x	x
Dol + Per + Cal + Fo	impossible	WD: 1140–3640 ND: >3640	<1260	o	?	WD	o
Dol + Brc + Cal + Fo	impossible	impossible	>1260	o	o	o	o
Dol + Qtz + Di	<2%	<3.4	<37	o	o	o	o
Di + Dol	<11%	<235	<46	o	o	o	o
Tlc + Dol + Cal	>14%	>91	>140	x	?	o	x
Tr + Dol + Cal	>9%	>75	>37	x	x	x	x
Per + Fo + Cal	impossible	>1890	no limit	x	?	x	o
Brc + Fo + Cal	impossible	impossible	>1090	o	o	o	o

* Limits are on the amount of fluid that stabilizes each mineral assemblage for the three models of fluid-rock interaction. Constant ϕ = constant porosity model (in percentages); Up-T flow = model for fluid flow in the direction of increasing temperature (time-integrated flux in moles of fluid per squared centimeter of rock); Down-T flow = model for fluid flow in the direction of decreasing temperature (mol/cm²). WD = stabilization of assemblage over a wide distance interval ($Z > 5$ m); ND = stabilization of the mineral assemblage over a narrow distance interval ($Z < 5$ m).

** Observed mineral assemblages: o = not observed; x = observed; WD = assemblage observed with wide spatial distribution; ? = occurrence uncertain either because of lack of information or because of ambiguous mineral identification.

TABLE 2. Assemblages developed in siliceous dolomitic limestone, model rock composition KSD, and limits on their conditions of formation

Assemblage	Limits*			Observed occurrences**	
	Constant ϕ	Up-T flow	Down-T flow	Marysville	Boulder
Dol + Qtz + Phl + Tr + Cal + Kfs	<18%	<260	140	x	o
Dol + Qtz + Tr + Di + Cal + Kfs	<15%	<195	20	x	o
Dol + Kfs + Phl + Cal + Qtz	no limit	WD: <865 ND: >865	>140	WD	WD
Dol + Qtz + Tr + Cal + Kfs	<16%	<195	20–140	x	WD
Dol + Qtz + Di + Kfs + Cal	<4%	<8.3	<20	o	o
Tr + Cal + Qtz + Di + Kfs	>4%	WD: 330–2500 ND: 195–330; >2500	WD: 3.5–23 ND: >23	WD	x
Dol + Qtz + Tr + Cal + Phl	>15%	WD: 135–1340 ND: >1340	>140	o	o
Phl + Cal + Qtz + Tr + Kfs	>16%	WD: 270–1720 ND: 260–270; >1720	>120	WD	x
Cal + Qtz + Wo + Di + Kfs	WD: >4% ND: <4%	WD: 240–3340 ND: <240; >3340	no limit	o	o
Kfs + Di + Cal + Phl + Wo	impossible	WD: 1190–4380 ND: >4380	no limit	o	o
Phl + Dol + Cal + Qtz	>15%	>98	>140	x	x
Phl + Tr + Cal + Qtz	>18%	>260	>120	x	o
Kfs + Tr + Cal + Qtz	>15%	>145	>20	x	o
Kfs + Wo + Di + Phl	impossible	>1640	no limit	o	o

* Limits are on the amount of fluid that stabilizes each mineral assemblage for the three models of fluid-rock interaction. Constant ϕ = constant porosity model (porosity in percentages); Up-T flow = model for fluid flow in the direction of increasing temperature (time-integrated flux in moles of fluid per squared centimeter of rock); Down-T flow = model for fluid flow in the direction of decreasing temperature (mol/cm²). WD = stabilization of assemblage over a wide distance interval ($Z > 5$ m); ND = stabilization of the mineral assemblage over narrow distance interval ($Z < 5$ m).

** Observed mineral assemblages: o = not observed; x = observed; WD = assemblage observed with wide spatial distribution.

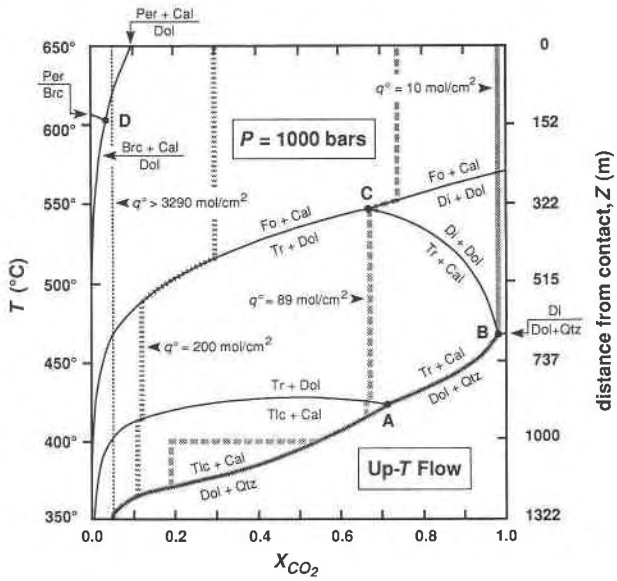

Fig. 10. Same as for Fig. 1 but with the dotted and thick shaded curves representing peak T-X_{CO_2} conditions when fluid flows in the direction of increasing temperature for different values of time-integrated input fluid flux (q^0). See text for details. The step on the trajectory for $q^0 = 89$ mol/cm² results from the corresponding constant q^0 path in Fig. 5 traversing the trough on the upper boundary to the Dol + Qtz + Tlc + Cal field.

is a sensitive function of ϕ and q when there is either no flow or down-temperature flow (Figs. 3 and 7). Likewise, the diopside isograd that corresponds to the boundary between the Tr + Dol + Cal and Di + Dol fields is a sensitive function of q when fluid flows up-temperature (Fig. 5).

***T*-X_{CO_2} diagrams.** For a given value of ϕ or q^0, peak conditions of contact metamorphism in the model aureole can be represented by a unique trajectory through an isobaric T-X_{CO_2} diagram. These trajectories illustrate conditions at the conclusion of metamorphism either at constant porosity and no flow or after influx and throughput of a given time-integrated input fluid flux, q^0. For the case of no fluid flow, the trajectories additionally illustrate how X_{CO_2} evolves at each position, Z, during progressive metamorphism. Where lines of constant ϕ or q^0 cross isobaric univariant fields in Figures 3–8, X_{CO_2} follows one of the T-X_{CO_2} curves in Figures 1 and 2. The temperature interval over which the T-X_{CO_2} curve is followed is read from the top horizontal axis of Figures 3–8. For the cases of no flow and up-temperature flow, X_{CO_2} is fixed along lines of constant ϕ or q^0 across isobaric divariant fields at the value of the high-temperature end of the univariant field immediately at lower temperature (greater Z). For the case of down-temperature flow, X_{CO_2} is fixed across divariant fields at the value of the univariant curve immediately at higher temperature (smaller Z). Selected T-X_{CO_2} trajectories for contact-metamorphosed siliceous dolomite are illustrated in Figures 1, 10, and 11 for the cases of no flow, up-temperature flow, and down-temperature flow, respectively. Figure 2 illustrates a more limited selection of T-X_{CO_2} trajectories for contact metamorphosed equivalents of the Kfs + Dol + Cal + Qtz rock.

If either ϕ or q^0 is small, fluids are driven to very CO_2-rich compositions by the metamorphic decarbonation reactions. When there is no flow or up-temperature flow, peak values of X_{CO_2} increase toward the pluton; when there is down-temperature flow, X_{CO_2} increases away from the pluton (Figs. 1, 2, 10, and 11). As porosity or time-integrated flux increases, the change in fluid composition is progressively less. For up-temperature flow and values of $q^0 > 3290$ mol/cm² in the case of the initial Dol + Qtz rock and of $q^0 > 3860$ mol/cm² in the case of the initial Kfs + Dol + Cal + Qtz rock, the entire flow system equilibrates with the input fluid, and the peak T-X_{CO_2} trajectory corresponds to a vertical line at constant $X_{CO_2} = 0.05$. For down-temperature flow and values of $q^0 > 2000$–3000 mol/cm², peak fluid composition over the entire flow system is H_2O rich ($X_{CO_2} < 0.1$). Taken together, Figures 1, 2, 10, and 11 illustrate that sequences and spatial distributions of mineral assemblages observed in a contact aureole are linked in different ways to peak T-X_{CO_2} paths inferred from mineral-fluid equilibria depending on the nature of fluid-rock interaction during metamorphism.

Progressive and nonprogressive contact metamorphism. Figures 3–8 contain information about the evolution of mineral assemblages during prograde contact metamorphism. With constant porosity and absence of fluid flow, the rock evolves mineralogically with increasing temperature along a horizontal path leftward from the right margins of Figures 3 and 4. Consideration of horizontal paths for same value of ϕ but to different peak temperatures shows that metamorphism at a constant porosity without fluid flow is progressive. All high-grade mineral assemblages develop from mineral assemblages that are preserved as peak assemblages at lower grades. When metamorphism involves fluid flow, time-integrated flux serves as a kind of clock: mineralogy evolves along upwardly directed paths in Figures 5–8. Consideration of vertical paths at different values of Z leads to the conclusion that high-grade mineral assemblages do not necessarily develop from peak assemblages preserved at lower grades when metamorphism involves fluid flow. As an example, consider an aureole composed of the Dol + Qtz rock that experiences prograde metamorphism with $q^0 = 5000$ mol/cm² and up-temperature flow (Fig. 5). Rock at $Z = 50$ m evolves from an early Fo + Dol + Cal assemblage to Dol + Per + Cal + Fo to Per + Fo + Cal; the rock never develops peak assemblages like Tr + Dol + Cal and Tlc + Dol + Cal that are preserved at lower grades (greater Z along the top dotted curve). The conclusion is valid regardless of whether the rock initially contains no porosity or a small ($\leq 1\%$) fluid-filled porosity. Metamorphism driven by fluid flow, either up- or down-temperature, may not be progressive even in systems that attain local equilibrium at all points in space and time.

Prograde hydration and carbonation reactions. An initial Di + Dol assemblage in the model Dol + Qtz rock converts to Tr + Dol + Cal in the interval Z = 333–663 m if progressive metamorphism involves either up- or down-temperature fluid flow (Figs. 5 and 7). During up-temperature flow, early-formed Tr + Dol + Cal later reacts to Tlc + Dol + Cal in the interval Z = 863–876 m (Fig. 5). Similarly an initial Kfs + Di + Cal + Qtz assemblage in the model Kfs + Dol + Cal + Qtz rock converts to Kfs + Tr + Cal + Qtz in the interval Z = 563–663 m if progressive metamorphism involves either up- or down-temperature flow (Figs. 6 and 8). During up-temperature flow, early-formed Kfs + Tr + Cal + Qtz later reacts to Phl + Tr + Cal + Qtz in the interval Z = 775–785 m (Fig. 6). When metamorphism is driven by infiltration, prograde reactions may involve hydration and carbonation, transforming what traditionally would be considered a high-grade assemblage to a low-grade assemblage. Uncritical interpretation of textural evidence for these reactions might erroneously attribute them to retrograde metamorphic processes.

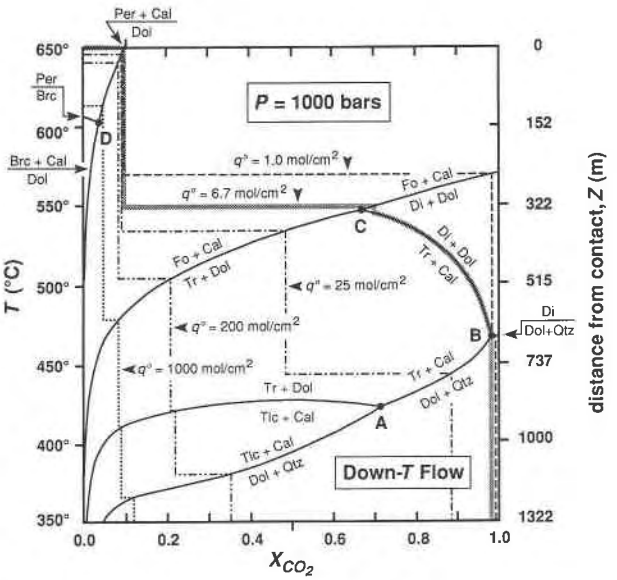

Fig. 11. Same as for Fig. 1 but with the shaded, dashed, dotted, and dash-dotted curves representing peak T-X_{CO_2} conditions when fluid flows in the direction of decreasing temperature for different values of time-integrated input fluid flux (q^0). See text for details.

Applications

Case studies in contact metamorphism of siliceous carbonate rocks

To the extent that the pressure, temperature profile, and bulk rock compositions in the model calculations are adequate approximations to those that existed during specific instances of contact metamorphism, observed mineral assemblages provide constraints on the nature of metamorphic fluid-rock interaction and the amount of fluid involved. Data for seven aureoles are reviewed; Tables 1 and 2 list observed diagnostic mineral assemblages and appropriately correlate the assemblages with calculated results for the three models of fluid-rock interaction. Although these correlations allow qualitative conclusions to be drawn with reasonable certainty, the quantitative conclusions are more tentative. Meaningful assessment of the accuracy of the quantitative interpretations, however, is impossible without more information about bulk rock compositions, modal abundances, spatial distributions of assemblages, and peak metamorphic temperatures in individual aureoles.

Beinn an Dubhaich aureole, Scotland. Assemblages listed in this paper are from the southeast portion of the contact aureole where bulk rock composition most closely matches the model Dol + Qtz rock (Holness, 1990, 1992). Widespread occurrence of the isobaric univariant assemblages Tr + Dol + Fo + Cal and Dol + Qtz + Tlc + Cal and the occurrence of the invariant assemblage Dol + Qtz + Tlc + Tr + Cal rule out down-temperature flow in the olivine zone and at lower grades. If there were no flow, the absence of the univariant assemblage Di + Dol + Fo + Cal near the forsterite isograd would require very large porosity, $\phi > 29\%$; metamorphism with no fluid flow therefore seems unlikely. For up-temperature fluid flow, the absence of Dol + Qtz + Di requires $q > 3.4$ mol/cm², whereas the occurrence of Dol + Qtz + Tr + Cal limits q to <100 mol/cm², at least in some parts of the tremolite zone. The absence of Di + Dol + Fo + Cal, however, requires $q > 240$ mol/cm² at or near the forsterite isograd. Fluid flow may have been spatially heterogeneous. The most commonly observed distribution of reactants and products in the talc (Reaction 3), tremolite (Reaction 10), and olivine (Reaction 11) zones could be explained by up-temperature fluid flow and $q^0 \approx 200$ mol/cm² (Fig. 5). The value is tentative, however, because the compressed spacing of isograds (Tr and Fo isograds are typically 200–250 m apart) implies a metamorphic temperature gradient steeper than that prescribed by Equation 1.

The occurrence of Per + Fo + Cal without Dol in the innermost 20 m of the aureole, however, is incompatible with up-temperature flow and $q^0 = 200$ mol/cm² (Fig. 5). Fluid flow in the innermost part of the aureole either was subhorizontal and directed away from the contact or was vertical. An O isotope study of the periclase zone could distinguish the two possibilities. The absence of primary brucite limits any subhorizontal down-temperature flow to $q < 1260$ mol/cm².

Alta aureole, Utah. The massive dolomites have compositions like the model Dol + Qtz rock (Moore and Kerrick, 1976). If the single occurrence of Dol + Qtz + Tlc + Cal in massive dolomites in the middle of the talc zone is representative, down-temperature flow in the outer portion of the aureole is unlikely. If there were no flow, the development of forsterite by Reaction 11 and the absence of Di + Dol + Fo + Cal near the forsterite isograd would limit porosity to >14 and >29%, respectively. Up-

temperature flow in the talc, tremolite, and forsterite zones seems more likely. The occurrence of Dol + Qtz + Tlc + Cal in the middle of the talc zone places an upper limit on q of 760 mol/cm^2; the absence of Di + Dol + Fo + Cal near the forsterite isograd requires $q > 240$ mol/cm^2. Up-temperature fluid flow and time-integrated input fluid flux of $\approx$200 mol/cm^2 could explain the inferred prograde sequence of mineral reactions in the talc (Reaction 3), tremolite (Reaction 10), and forsterite (Reaction 11) zones but not in the periclase zone (Fig. 5).

O isotope data indicate layer-parallel, subhorizontal, down-temperature fluid flow in the periclase zone with average $q \approx 1000$ mol/cm^2 (Bowman et al., 1994). The value is fully consistent with the position of the periclase isograd 100–150 m from the contact in the southern part of the aureole (Moore and Kerrick, 1976) predicted from the model for horizontal, down-temperature flow (Fig. 7). If q were much larger, primary brucite would be expected. Interestingly, if the occurrence of Dol + Qtz + Tlc + Cal is unrepresentative and isobaric univariant assemblages are rare in the aureole, positions of the forsterite, tremolite, and talc isograds could also be explained by down-temperature flow and $q^0 \approx 1000$ mol/cm^2 (Fig. 7).

Notch Peak aureole, Utah. Detailed comparison between observed assemblages and model calculations is meaningless because siliceous dolomitic limestones contain abundant calcite with minor dolomite and quartz. Regardless of rock composition, however, the absence of periclase (Hover-Granath et al., 1983) rules out down-temperature fluid flow into the limestones at the contact. Any flow of magmatic fluid into the aureole, as proposed by Nabelek et al. (1984) and Labotka et al. (1988), must have been restricted to the argillaceous layers.

Kasuga-mura aureole, Japan. Within the context of the model Dol + Qtz rock, (1) occurrences of the isobaric invariant assemblages Dol + Qtz + Tlc + Tr + Cal and Dol + Qtz + Tr + Di + Cal, (2) widespread occurrences of the univariant assemblages Dol + Qtz + Tlc + Cal, Dol + Qtz + Tr + Cal, and Tlc + Cal + Tr + Dol, and (3) an absence of periclase at the contact makes the likelihood of down-temperature flow anywhere in the aureole remote (Suzuki, 1977). If there were no flow, occurrences of Tlc + Dol + Cal would require an unlikely $\phi > 14\%$. Up-temperature flow is more plausible. The absence of Dol + Qtz + Di and periclase then limits q to 3–1140 mol/cm^2 over the whole aureole. Occurrences of Dol + Qtz + Tr + Cal locally require $q < 100$ mol/cm^2, whereas the widespread occurrence of Tlc + Cal + Tr + Dol requires $q = 170$–920 mol/cm^2 in other parts of the aureole. Fluid flow may have been spatially heterogeneous.

Elkhorn aureole, Montana. Bowman and Essene (1982) reported a prograde sequence in siliceous dolomites of Dol + Qtz to Tr + Dol + Cal (tremolite zone) to Fo + Dol + Cal (forsterite zone) to Dol + Per + Cal + Fo (periclase zone). Isobaric invariant assemblages are absent, and (except in the periclase zone) univariant assemblages are either absent or restricted to the boundary between zones. The only model that can explain the observed sequence of minerals in the tremolite and forsterite zones is down-temperature fluid flow with $q = 37$–165 mol/cm^2 at the tremolite isograd. The entire prograde sequence could have been produced by a time-integrated input fluid flux, $q^0 \approx 25$ mol/cm^2 (Fig. 7). The value is tentative, however, because the greatly telescoped spacing of isograds (all within $\approx$100 m of the contact) implies a metamorphic temperature gradient much steeper than that prescribed by Equation 1. Widespread occurrence of Dol + Per + Cal + Fo in the periclase zone is inconsistent with horizontal down-temperature flow near the contact (Per + Fo + Cal would be expected). The conclusion is substantiated by the lack of an O isotope alteration front in the periclase zone: isotopically nearly unaltered dolomite is observed within $\approx$1 cm of the contact (Bowman et al., 1985). The isotopic and petrologic data indicate vertical flow in dolomites near the contact, consistent with the study of adjacent skarn deposits (Bowman et al., 1985).

Marysville and Boulder aureoles, Montana. The model Dol + Qtz + Cal + Kfs rock approximates the composition of siliceous dolomitic limestones examined by Rice (1977a, 1977b). Occurrence of the isobaric invariant assemblages Dol + Qtz + Phl + Tr + Cal + Kfs and Dol + Qtz + Tr + Di + Cal + Kfs at Marysville and the widespread occurrence of the univariant assemblages Dol + Qtz + Tr + Cal + Kfs (Boulder), Tr + Cal + Qtz + Di + Kfs and Phl + Cal + Qtz + Tr + Kfs (Marysville), and Dol + Kfs + Phl + Cal + Qtz (Boulder and Marysville) rules out down-temperature fluid flow. If there were no fluid flow, occurrences of Phl + Tr + Cal + Qtz and Kfs + Tr + Cal + Qtz at Marysville and Phl + Dol + Cal + Qtz at both localities would require $\phi > 15\%$. Up-temperature fluid flow seems more plausible. Values of q in the range 8–865 mol/cm^2 explain the observed prograde sequence of assemblages and inferred mineral reactions in zones A (Dol + Kfs + Phl + Cal + Qtz, Phl + Dol + Cal + Qtz), B (Dol + Qtz + Tr + Cal + Kfs, Phl + Cal + Qtz + Tr + Kfs, Phl + Tr + Cal + Qtz, Kfs + Tr + Cal + Qtz), and C (Tr + Cal + Qtz + Di + Kfs, Kfs + Di + Cal + Qtz) of the Boulder and Marysville aureoles and in zone D (Kfs + Di + Cal + Qtz) at Marysville. The sequence could be produced by a time-integrated input fluid flux, $q^0 \approx 200$ mol/cm^2 (Fig. 6). In zone B the assemblage Dol + Qtz + Tr + Cal + Kfs locally requires $q < 195$ mol/cm^2, whereas the occurrence of Phl + Cal + Qtz + Tr + Kfs locally requires $q > 260$ mol/cm^2. Fluid flow may have been spatially heterogeneous.

Generalizations from case studies

Geometry of fluid flow. The contact aureoles listed in Tables 1 and 2 contain mineral assemblages requiring implausibly large synmetamorphic porosities of >14% if metamorphism was not accompanied by fluid flow. Occurrences of isobaric invariant and univariant assemblages in five aureoles make the possibility of horizontal, down-temperature fluid flow unlikely in the outer portions of the aureoles. Formation of periclase at several localities, however, is best explained by down-temperature flow near the contact. In many aureoles fluid prob-

ably flowed up-temperature toward the pluton at distances $> \approx 100$ m from the contact and down-temperature at distances $< \approx 100$ m. The absence of periclase at Notch Peak and Kasuga-mura indicates that the inner, down-temperature flow system is not universally present. Contact metamorphism at Elkhorn, Montana, is an exception to these generalizations. At the present level of exposure, fluid flow was directed away from the pluton in the outer portions of the aureole and was vertical near the contact. Fluid-flow geometries of contact metamorphism evidently are diverse.

Quantity of fluid. Within the context of model calculations, tentative generalizations can be made about the amount of fluid involved in contact metamorphism of siliceous carbonate rocks. Because primary brucite is never observed, the inner flow systems, where present, involve $q < 1300$ mol/cm^2. A lower limit on $q \approx 10$ mol/cm^2 in the outer portions of the aureoles is set by the universal absence of Dol + Qtz + Di in isobaric univariant assemblages. An upper limit of ≈ 800 mol/cm^2 is provided by the widespread distribution of the low-grade isobaric univariant assemblages Dol + Qtz + Tlc + Cal and Dol + Kfs + Phl + Cal. The small estimated values of time-integrated flux are fully consistent with the absence of significant O isotope alteration in the outer portions of the aureoles (e.g., Nabelek et al., 1984; Bowman et al., 1994). Up-temperature fluid flow results in measurable isotopic effects (> 1‰) only when time-integrated fluxes are > 2000 mol/cm^2 (Dipple and Ferry, 1992).

Fluid flow and heat transfer. Given an average time-integrated fluid flux of ≤ 1000 mol/cm^2, fluid with composition $X_{CO_2} = 0.5$ at 500 °C and 1 kbar, and a flow time of ≥ 2000 yr, the average fluid flux during contact metamorphism is $\leq 10^{-8}$ m/s. For fluid flux in this range, transport of heat by fluid flow in kilometer-sized contact aureoles is negligible (Bickle and McKenzie, 1987).

Acknowledgments

This paper was written during sabbatical leave at the Department of Earth Sciences, University of Cambridge. I thank J. Baker, M. Bickle, M. Carpenter, H. Chapman, and T. Holland for discussion and hospitality. The manuscript benefited from critical reviews by T.D. Hoisch, T.C. Labotka, and D. Perkins. Research was supported by the National Science Foundation, Division of Earth Sciences, grant EAR-910484.

References cited

Baumgartner, L.P., and Ferry, J.M. (1991) A model for coupled fluid-flow and mixed-volatile mineral reactions with applications to regional metamorphism. Contributions to Mineralogy and Petrology, 106, 273–285.

Berman, R.G. (1988) Internally-consistent thermodynamic data for minerals in the system Na_2O-K_2O-CaO-MgO-FeO-Fe_2O_3-Al_2O_3-SiO_2-TiO_2-H_2O-CO_2. Journal of Petrology, 29, 445–522.

Bickle, M., and Baker, J. (1990) Migration of reaction fronts in infiltration zones: Assessments of fluid flux in metamorphic terrains. Earth and Planetary Science Letters, 98, 1–13.

Bickle, M.J., and McKenzie, D. (1987) The transport of heat and matter by fluids during metamorphism. Contributions to Mineralogy and Petrology, 95, 384–392.

Bowman, J.R., and Essene, E.J. (1982) P-T-$X(CO_2)$ conditions of contact metamorphism in the Black Butte aureole, Elkhorn, Montana. American Journal of Science, 282, 311–340.

Bowman, J.R., O'Neil, J.R., and Essene, E.J. (1985) Contact skarn formation at Elkhorn, Montana. II. Origin and evolution of C-O-H skarn fluids. American Journal of Science, 285, 621–660.

Bowman, J.R., Willett, S.D., and Cook, S.J. (1994) Oxygen isotopic transport and exchange during fluid flow: One-dimensional models and applications. American Journal of Science, 294, 1–55.

Bucher-Nurminen, K. (1982) On the mechanism of contact aureole formation in dolomitic country rock by the Adamello intrusion (northern Italy). American Mineralogist, 67, 1101–1117.

Dipple, G.M., and Ferry, J.M. (1992) Fluid flow and stable isotopic alteration in rocks at elevated temperatures with applications to metamorphism. Geochimica et Cosmochimica Acta, 56, 3539–3550.

Ferry, J.M. (1991) Dehydration and decarbonation reactions as a record of fluid infiltration. In Mineralogical Society of America Reviews in Mineralogy, 26, 351–393.

Ferry, J.M., and Dipple, G.M. (1992) Models for coupled fluid flow, mineral reaction, and isotopic alteration during contact metamorphism: The Notch Peak aureole, Utah. American Mineralogist, 77, 577–591.

Furlong, K.P., Hanson, R.B., and Bowers, J.R. (1991) Modeling thermal regimes. In Mineralogical Society of America Reviews in Mineralogy, 26, 437–505.

Hanson, R.B. (1992) Effects of fluid production on fluid flow during regional and contact metamorphism. Journal of Metamorphic Geology, 10, 87–97.

Holness, M.B. (1990) Experimental and petrological studies of textural equilibration and fluid flow in metacarbonate rocks: The Beinn an Dubhaich aureole, Skye, 216 p. Ph.D. thesis, University of Cambridge, Cambridge, U.K.

——— (1992) Metamorphism and fluid infiltration of the calc-silicate aureole of the Beinn an Dubhaich granite, Skye. Journal of Petrology, 33, 1261–1293.

Hover-Granath, V.C., Papike, J.J., and Labotka, T.C. (1983) The Notch Peak contact metamorphic aureole, Utah: Petrology of the Big Horse Limestone Member of the Orr Formation. Geological Society of America Bulletin, 94, 889–906.

Kerrick, D.M., and Jacobs, G.K. (1981) A modified Redlich-Kwong equation for H_2O, CO_2, and H_2O-CO_2 mixtures at elevated pressures and temperatures. American Journal of Science, 281, 735–767.

Labotka, T.C., White, C.E., and Papike, J.J. (1984) The evolution of water in the contact-metamorphic aureole of the Duluth Complex, northeastern Minnesota. Geological Society of America Bulletin, 95, 788–804.

Labotka, T.C., Nabelek, P.I., and Papike, J.J. (1988) Fluid infiltration through the Big Horse Limestone Member in the Notch Peak contact-metamorphic aureole, Utah. American Mineralogist, 73, 1302–1324.

Lasaga, A.C., and Rye, D.M. (1993) Fluid flow and chemical reaction kinetics in metamorphic systems. American Journal of Science, 293, 361–404.

Marsh, B.D. (1981) On the crystallinity, probability of occurrence, and rheology of lava and magma. Contributions to Mineralogy and Petrology, 78, 85–98.

Moore, J.N., and Kerrick, D.M. (1976) Equilibria in siliceous dolomites of the Alta aureole, Utah. American Journal of Science, 276, 502–524.

Nabelek, P.I., Labotka, T.C., O'Neil, J.R., and Papike, J.J. (1984) Contrasting fluid/rock interaction between the Notch Peak granitic intrusion and argillites and limestones in western Utah: Evidence from stable isotopes and phase assemblages. Contributions to Mineralogy and Petrology, 86, 25–34.

Norton, D., and Knight, J. (1977) Transport phenomena in hydrothermal systems: Cooling plutons. American Journal of Science, 277, 421–486.

Rice, J.M. (1977a) Progressive metamorphism of impure dolomitic limestone in the Marysville aureole, Montana. American Journal of Science, 277, 1–24.

——— (1997b) Contact metamorphism of impure dolomitic limestone in the Boulder aureole, Montana. Contributions to Mineralogy and Petrology, 59, 237–259.

Rice, J.M., and Ferry, J.M. (1982) Buffering, infiltration, and the control

of intensive variables during metamorphism. In Mineralogical Society of America Reviews in Mineralogy, 10, 263–326.

Suzuki, K. (1977) Local equilibrium during the contact metamorphism of siliceous dolomites in Kasuga-mura, Japan. Contributions to Mineralogy and Petrology, 61, 79–89.

Taylor, H.P., Jr. (1977) Water/rock interaction and the origin of H_2O in granitic batholiths. Journal of the Geological Society of London, 133, 509–558.

Turcotte, D.L., and Schubert, G. (1982) Geodynamics: Applications of continuum physics to geological problems, 450 p. Wiley, New York.

Manuscript received July 12, 1993
Manuscript accepted March 4, 1994